EDGE ARTICLE

Insights into the photoinduced anion translocation of donor–π–acceptor+ (ion)− molecules†

Hao-Ting Qu, [ID] [a] Iida Partanen,[b] Kai-Hsin Chang, [ID] [a] Yan-Ding Lin,[a] Igor O. Koshevoy, [ID] *[b] Andrey Belyaev [ID] *[bc] and Pi-Tai Chou [ID] *[a]

By strategic design and synthesis of a new series of phosphonium salts (compounds 1–7[OTf]), where [OTf]− stands for the trifluoromethanesulfonate anion, we performed comprehensive spectroscopic and dynamic studies on the photoinduced anion migration in toluene. Our aim is to probe if the anion migration is associated with an intrinsic barrier or is barrier-free. After the occurrence of excited-state intramolecular charge transfer (ESICT) in 1–7, the charge redistribution of the cation triggers the translocation of the counter anion [OTf]−, resulting in emission spectral temporal evolution. As a result, we describe the photoinduced anion migration by introducing spectral response function $C(t)$, a concept adopted from the solvent diffusional relaxation. The experimental results indicate that the anion migration lacks an intrinsic barrier, *i.e.*, the relaxation dynamics can be described by a biased Brownian motion along the charge transfer direction. The experimental findings are also qualitatively supported by theoretical calculations including restrained electrostatic potential (RESP) and hole−electron distribution analyses.

Introduction

Rational design of molecular machines that can accomplish sophisticated work in the nano-micro scale is always a challenge. On the one hand, bionic machines that mimic biological systems have been one research direction.[1,2] Specific stimulus–response behavior is conferred on them by their unique structural complexity. However, biological machines encounter instability and potential invalidation upon detachment from organisms.[3,4] On the other hand, artificial molecular machines provide a solution to these limitations. Over 50 years of development,[5] the well-established artificial molecular machines, for example, rotaxanes, have operated under various conditions such as in organic solvents[6] and polymer solutions,[7] on electrode surfaces,[8] or even in the solid state.[9] In light of the versatile operation environment, a great deal of applications have emerged.[10–14]

Fundamentally, how the motion of molecular machines is controlled is always of top interest. In solution, the motion of molecules is complicated by the Brownian motion, so the

imposition of a bias to change random mobility into a directional motion is a key.[3,15,16] In view of chemistry, how to break the equilibrium and make the given elementary reaction step move forward are pivotal. Take the rotaxane molecular shuttle as an example, which comprises a thread with two stoppers on the two sides and an interlocked macrocycle binding to one of the stations along the thread.[17,18] To extract effective work, the macrocycle in the stimuli–responsive molecular shuttles travels between two stations in response to external stimuli upon modifying the binding affinity of one of the stations. Aside from this, if the macrocycle originally accumulates at one of the identical stations and a compartment blocks the macrocycle shuttling between these two, once removing the barrier, the statistically unstable state would prompt the macrocycle to redistribute, and the overall reaction basically becomes irreversible.[15,16] Both types of molecular shuttles relax from an unbalanced state into a stable one and perform monodirectional motion. After harnessing the direction of molecular shuttles, the following dynamic study on them is necessary. In this regard, steady-state absorption spectra,[19] NMR spectra,[20] cyclic voltammetry,[8,9] transient infrared[21] or UV-vis[7,22] absorption spectra were adopted to monitor the conformation variation. For example, the hydrogen-bonded (H-bonded) molecular shuttles are a popular paradigm for quantifying the shuttle rate of a macrocycle by the time trace of a characteristic vibrational frequency shift[21] or time-resolved transient absorption feature.[22]

In 2019, our team initiated a seminal study associated with photoinduced anion migration of a series of D−π−A+ (anion)−

[a]Department of Chemistry, National Taiwan University, Taipei, 10617 Taiwan, Republic of China. E-mail: chop@ntu.edu.tw

[b]Department of Chemistry, University of Eastern Finland, Yliopistokatu 7, 80101 Joensuu, Finland. E-mail: igor.koshevoy@uef.fi; andrei.beliaev@uef.fi

[c]Department of Chemistry/Nanoscience Center, University of Jyväskylä, Survontie 9C, 40014 Jyväskylä, Finland. E-mail: andrei.a.beliaev@jyu.fi

push–pull systems (see Scheme 1),[23–26] where the electron acceptor is originally positively charged. In medium and high polar solvents, the salts exist as isolated ions with solvent shells surrounding the individual ions. In this scenario, excited-state intramolecular charge transfer (ESICT) shifts the electron density from the donor to the acceptor, altering the charge distribution. Fast solvent relaxation then takes place to stabilize the charge transfer state. In weakly polar solvents such as toluene or 1,4-dioxane, however, ion pairs are preferably formed due to poor solvent–solute interaction. Therefore, the role of stabilization switches from the surrounding solvent molecules to the counter anion. After ESICT, the positively charged acceptor receives the negative charge from the donor. The net result is to alleviate the coulombic interaction within the ion pair and allow the anion to translocate toward the donor site that becomes positively charged, in part, after ESICT. In the end, we achieve a directional anion shuttle from the electron acceptor to the donor site. Such an anion migration has been reported to be significantly slower than that of solvent relaxation. Therefore, broad and even multiple emissions can be observed along the time constant of anion migration. Upon relaxation to the ground state, an opposite directional shuttle should take place, achieving a reversible cycle of light induced anion migration (see Scheme 1). Ultimately, effective work in the excited state can only be extracted if the population decay lifetime is longer than the translocation time.[27] Tuning the excited state lifetime is thus crucial for future applications of these molecular machines, which is not the focus of this study.

Upon establishing the anion migration mechanism, a crucial issue lies in the kinetics of anion migration. It would be of both interest and importance to know whether such an anion translocation is a mass transport process, or a process related to an intrinsic, *i.e.*, a non-viscosity-induced, barrier. Also, if a barrier exists, could it be dependent on molecular structure, incorporating either the electron donor, the acceptor or even the bridge configuration? Aimed at answering these questions, in this study, we designed and synthesized a series of phosphonium triflate salts featuring certain electronic and structural modifications (Scheme 2). In view of chemical structure, we divide them into three groups. Group A involves the variation of the electron-donating properties of the amine fragment, while in group B the effect of the acceptor strength is probed. In group C, we alter the structure of the bridge to tune the dihedral
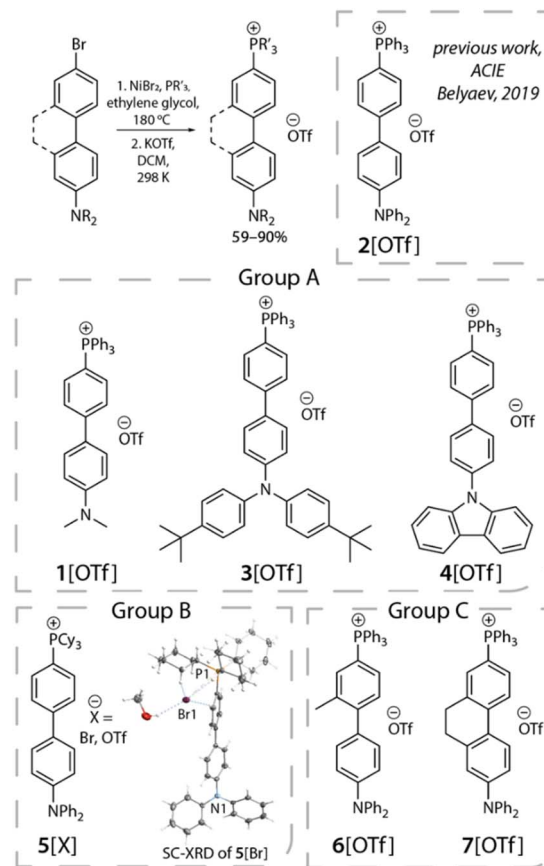
Scheme 2 General synthetic approach to phosphonium salts **1–7** [OTf] and their structure. Inset of group B shows the molecular view of **5[Br]** obtained by SC-XRD. Thermal ellipsoids are shown at the 50% probability level.

angle within the biphenyl group by introducing a planarity-restricting substituent or ring closure. To simplify the approach, all D–π–A$^+$ compounds are anchored with the same counter anion **[OTf]$^-$** (trifluoromethanesulfonate),[23] yielding compounds **1[OTf]** to **7[OTf]**. Although we have studied **2[OTf]** in 2019,[23] to ensure the completeness of the discussion regarding D/A electronic properties of these salts, we also include **2[OTf]** in the results for the later discussion. Our previous studies of time-resolved emission spectra (TRES) of **2 [OTf]** have unveiled the continuous spectral temporal evolution of emission bands, but have not yet quantified the trend of translocation dynamics. Inspired by the similar red-shifted behavior in spectra caused by the solvent relaxation, we employ the spectral response function $C(t)$, which is generally applied in solvatochromism studies, to extract valuable information regarding the dynamics of anion migration. To probe $C(t)$, we perform comprehensive time-resolved analyses, focusing on the anion translocation rate, which is viscosity-dependent and temperature-dependent. The comprehensive experimental work, together with the computational approach on the electrostatic potential, lead us to conclude that the rate of photoinduced anion migration in **1–7** can be described as an ion-mobility dependent mass transport process[28] caused by the
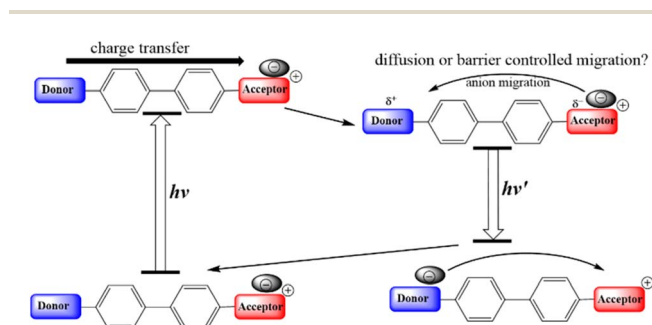
Scheme 1 The proposed photoinduced charge transfer associated with counter anion migration in weakly polar solvents.

change of the electric field. Details of results and discussion are elaborated in the following sections.

Results and discussion

Synthesis and characterization

Phosphonium salts **1–7[OTf]** were synthesized *via* an NiBr$_2$-catalyzed coupling arylation reaction between PPh$_3$ or PCy$_3$ and the corresponding donor-functionalized biphenyl bromide, followed by counterion metathesis with potassium triflate salt in dichloromethane (for more details, see the ESI†).[29] All the phosphonium species were isolated in good yields (59–90%). The composition of the products was confirmed by ^{31}P, ^{13}C and ^{1}H NMR spectra, which are compatible with the proposed structures and the presence of single species for each compound. The phosphorus resonances in CD$_2$Cl$_2$ appear in the narrow range of 23.3–23.8 ppm for **1–4**, **6–7[OTf]**, and 29.9 ppm for **5[X]** (X = Br, OTf). These chemical shifts are typical for other acyclic phosphonium compounds, which also reflect the accepting power of the cationic fragment.

The molecular structure of **5[Br]** was elucidated by SC-XRD analysis (Scheme 2 and Table S1†). The organic cation contains a twisted biphenyl fragment (torsion angle equals 21.4°), decorated by the diphenyl amine group and the phosphorus atom with nearly ideal tetrahedral geometry (∠C–P–C angles are between 107.8 and 108.6°, C–P bond lengths are 1.765–1.796 Å). The molecule represents a contact ion pair as a result of electrostatic attraction supported by a network of hydrogen bonds involving cyclohexyl fragments and Br counterions (H···Br distances fall in the range of 2.41–3.06 Å).

Photophysical steady-state spectroscopy

Fig. 1 shows the absorption and emission spectra of the studied salts in toluene, while those measured in other solvents are depicted in Fig. S2.† All pertinent steady-state data are listed in Tables 1 and S2.† In polar aprotic solvents (chloroform, dichloromethane, acetonitrile), the lowest lying absorption band undergoes a hypsochromic shift with increasing polarity. This phenomenon has been well-documented in numerous reports[30–37] and is due to a larger dipole moment in the ground than that of the Franck–Condon excited state. The ESICT

Fig. 1 The steady-state spectra of salts **1[OTf]**, **3–7[OTf]** in toluene. Absorption and emission spectra are depicted in dashed and solid lines, respectively.

properties of **1–7** are manifested by the structureless and polarity-sensitive emission bands in terms of peak wavelength. This assignment is also supported by the hole–electron analysis,[38] where hole and electron distributions are separated and located at the electron donor and acceptor (the phosphonium group), respectively (Fig. S14–S15 and Tables S10–S11†). In medium and strong polar solvents, the emission spectra of **1–7** exhibit a bathochromic shift upon increasing the solvent polarity (see Fig. S2†).

In weakly polar solvents such as toluene, all studied compounds show broad emission profiles composed of at least two components (see Fig. 1). For the convenience of discussion, as for the dual emission, the short- and long-wavelength emissions are assigned to the F$_1$ and F$_2$ bands, respectively. The high-energy F$_1$ band specifies the emission of the species where the anion stays near the phosphonium acceptor. Meanwhile, low-energy F$_2$ corresponds to the state formed by the anion migration from the phosphonium group to the donor. Later, we will show that this process is driven by the change of electrostatic potential arising from the charge transfer in the excited state, leading to the system stabilization (*vide infra*).

Time-resolved spectroscopy

We then focus on the dynamics of the anion migration in toluene, where this phenomenon is associated with the temporal spectral evolution from short-(F$_1$) to long-(F$_2$) wavelength. The wavelength-variable fluorescence time trace was measured by the time-correlated single photon counting (TCSPC). Our current setup of TCSPC incorporates a 120 fs Ti-sapphire laser and microchannel plates, giving a time resolution of around 15–20 ps. This response time is short enough to resolve the anion translocation processes, which have been reported to be within a time constant of several hundred picoseconds.[23–26] TCSPC, though having a longer response time than that of the fluorescence up-conversion technique currently available in our lab, provides stable spectral measurements due to the weak excitation intensity and low noise level.

To obtain meaningful time-resolved emission spectra, we employed the method described in the literature,[41] where the spectra at various delay times were plotted with the area of each spectrum normalized to a constant value. Please see the ESI for details.† As shown in Fig. 2(a), upon excitation at the absorption peak, in toluene these compounds initially exhibit prominent emissions maximized at ∼460 (**2[OTf]**), 485 (**3[OTf]**) and 430 nm (**4[OTf]**). As the time evolves, the signals gradually red shift and eventually appear as new bands centered at ∼580, 630 and 525 nm, respectively. Note that the spectra are plotted under the condition that area of entire spectrum is normalized to a constant value. Similar type of plotting methodology has been reported.[41] Throughout the whole spectral evolution, the absence of definite iso-emissive point indicates the existence of more than two emitting species. Similar phenomena are observed for **5–7[OTf]** (see Fig. S5(a)†). In other words, the results should be described more specifically by the continuous spectral evolution rather than interconversion of two species.[23–26] Due to the continuous character of the changes in
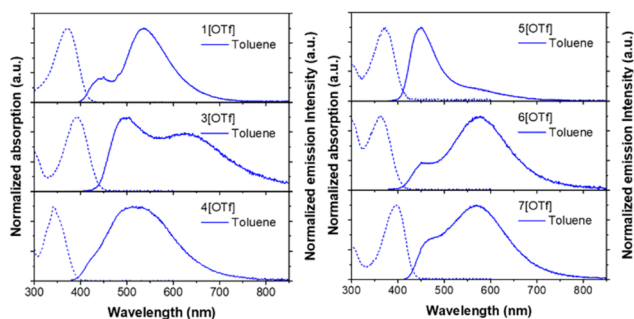
Table 1 Photophysical properties of **1–7[OTf]** in toluene (298 K)[a]

	Computational			Experimental			
	λ_{abs} (nm)	λ_{em} (nm)	HOMO/LUMO (eV)	λ_{abs} (nm)	λ_{em} (nm)	Stokes shift (cm^{-1})	PLQY
1[OTf]	353	399	−7.28/−2.31	371	438, 540	8436	0.14
2[OTf]	363	435	−7.12/−2.20	383	475, 587	9074	0.17
3[OTf]	379	456	−6.96/−2.35	391	493, 619	9420	0.16
4[OTf]	330	403	−7.45/−2.31	341	429, 475, 532	10 529	0.59
5[OTf]	359	428	−7.11/−2.02	370	450, 516	7647	0.91
6[OTf]	348	420	−7.11/−2.15	363	455, 573	10 096	0.40
7[OTf]	380	439	−7.08/−2.35	397	464, 566	7521	0.49

[a] λ_{abs} and λ_{em} are absorption and emission peak wavelengths, respectively, accessed by computational calculations and steady-state spectroscopies. The calculations including the HOMO/LUMO level are based on DFT/TDDFT with M06-2x/6-31G+(d,p).[39,40] The experimental λ_{em} is given by Gaussian function deconvolution (Fig. S3). The Stokes shift is defined by the difference between the absorption and longest emission peak in terms of frequency. PLQY is the photoluminescence quantum yield. For details of derivation of PLQY, please see the ESI.

time, it is therefore not possible to have a single exponential decay in the early dynamics for a given emission wavelength. Nevertheless, in a qualitative manner, upon monitoring the intensity at the peak of the F_2 band and fitting the rise component with a single exponential function, we obtain a rise time constant in the order of **1[OTf]** < **2[OTf]** < **3[OTf]** < **4[OTf]** for group A, **2[OTf]** < **5[OTf]** for group B and **6[OTf]** < **2[OTf]** < **7 [OTf]** for group C (see Table 2). These trends are consistent with the prediction that increasing electron donor or acceptor strength will enhance the positive charge to localize at the donor site, hence reducing the time constant of the anion migration, *i.e.*, accelerating the anion translocation (*vide infra*).

The observation of continuous spectral evolution of anion translocation reflects the general relaxation mechanism of polar solvents in the presence of emitters with charge transfer character. In such systems, electronic excitation changes the dipole moment with respect to the ground state in terms of magnitude and direction. Following this, the surrounding solvent molecules reorient their dipoles, thereby stabilizing the charge-transfer state. This solvent rearrangement also destabilizes the hot ground state formed upon vertical Franck–Condon transition. Therefore, the time-resolved Stokes shifted emission during the solvent relaxation can be described by the spectral response function $C(t)$ expressed in eqn (1) (ref. 42–50)
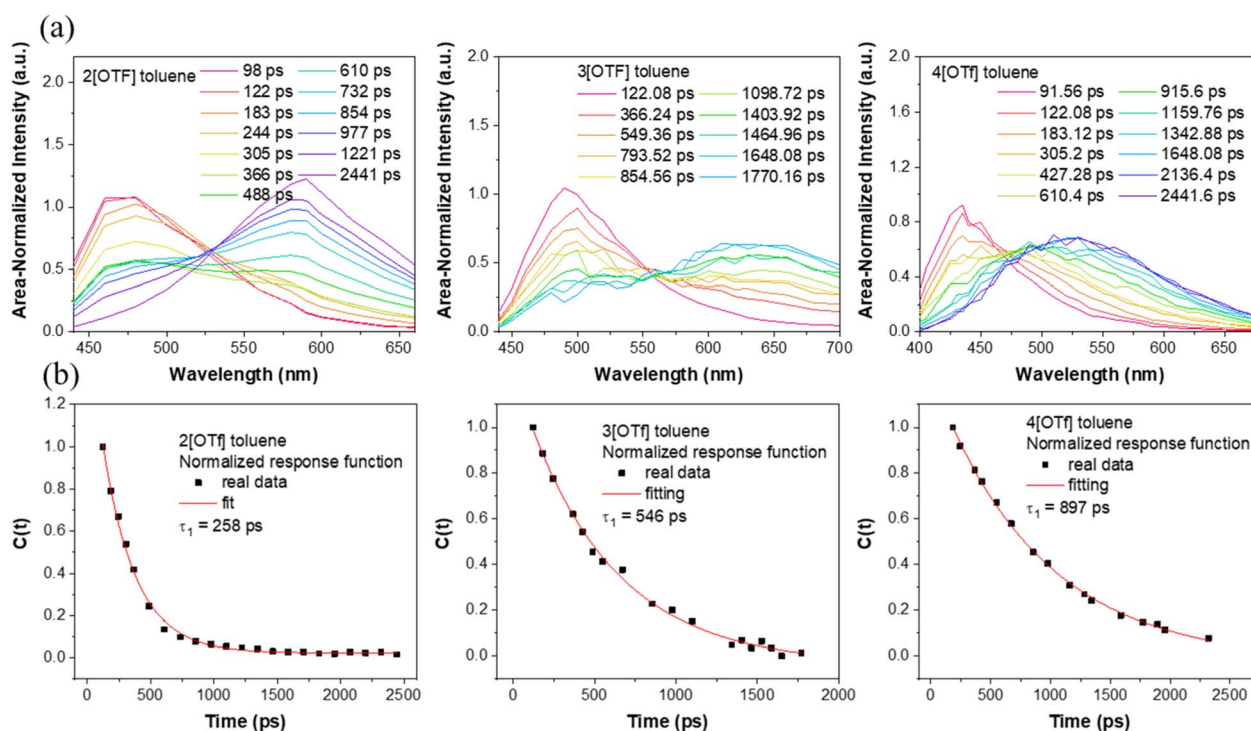

Fig. 2 (a) Time-resolved emission spectra of **2[OTf]**,[30] **3[OTf]**, and **4[OTf]**. Note that the spectra are plotted under the condition that the area of the entire spectrum is normalized to a constant value. A similar type of plotting methodology has been reported in ref. 41. (b) Spectral response functions $C(t)$ of **2[OTf]**, **3[OTf]**, and **4[OTf]** in toluene.

Table 2 Time-resolved parameters of **1–7[OTf]** in toluene (298 K)[a]

	τ_1 (ps) at F1	τ_2 (ps) at F2	τ_{trans}(ps)
1[OTf]	440 nm: 30 (0.82), 268 (0.18)	650 nm: 83 (−0.40), 1035 (0.60)	∼80 (from TCSPC)
2[OTf]	430 nm: 150 (0.73), 660 (0.27)	650 nm: 298 (−0.45), 3807 (0.55)	258
3[OTf]	440 nm: 24 (0.85), 583 (0.15)	660 nm: 378 (−0.45), 1587 (0.55)	546
4[OTf]	430 nm: 59 (0.64), 524 (0.34), 4741 (∼0)	650 nm: 519 (−0.43), 5906 (0.57)	897
5[OTf]	430 nm: 840 (0.65), 3165 (0.35)	650 nm: 931 (−0.49), 3415 (0.51)	1324
6[OTf]	430 nm: 51 (0.58), 388 (0.42), 4300 (∼0)	650 nm: 288 (−0.48), 4266 (0.52)	172
7[OTf]	430 nm: 376 (0.96), 2751 (0.04)	650 nm: 395 (−0.50), 3874 (0.50)	467

[a] τ_1 and τ_2 are the time constant measured by the TCSPC method. τ_{trans} represents the decay time constant obtained by the spectral response function $C(t)$. The value in parentheses is the pre-exponential factor from the lifetime fitting, and negative values indicate a rise component.

$$C(t) = \frac{\nu(t) - \nu(\infty)}{\nu(0) - \nu(\infty)} \qquad (1)$$

where $\nu(0)$ represents the frequency of the initial emission peak, $\nu(t)$ is the emission at any given time during the process, and $\nu(\infty)$ denotes the equilibrium emission peak.

Eqn (1) directly relates to the time evolution of the solvation free energy or solvent configuration in the vicinity of the ESICT molecule and is applicable to a variety of conditions.[45–49] The simplest model to describe the rotating solvent dipoles is the Debye–Onsager model,[42] where the $C(t)$ function becomes a single exponential function with a decay time constant called the solvent longitudinal relaxation time. Alternatively, for a more sophisticated model to approach reality, the $C(t)$ is non-exponential. An average relaxation time can be applied for the discussion, which is the value deduced by the integration of the $C(t)$.[51] These two values are used interchangeably, showing the same trend in the data interpretation.

Note that the above treatment requires solvent relaxation as the sole contribution to the entire relaxation process.[44,45] Due to the π-linkage between the donor and acceptor, the charge transfer of **1–7** should be ascribed to an adiabatic type, *i.e.*, a type of optical electron transfer. Hence the rate of charge transfer for **1–7** should be ultrafast (fs), which can be decoupled from the solvent relaxation (ps), fulfilling the criterion for eqn (1).[50] In a polar solvent (*e.g.*, CH$_2$Cl$_2$), eqn (1) should be applicable to the title compounds **1–7[OTf]**. Support of this viewpoint is given by the fluorescence up-conversion measurement of *e.g.*, **3[OTf]**, where the spectral response function $C(t)$ is depicted in Fig. S12,† with a longitudinal relaxation time fitted to be 1.24 ps, which is consistent with the reported value (1.02 ps).[48]

Differently, instead of solvent stabilization, here, we are dealing with the anion migration stabilizing cation chromophore after ESICT in the weakly polar solvent. Nevertheless, the resulting $C(t)$ (see Fig. 2) is still a single exponential-like decay. We thus propose that $C(t)$ may be applicable to the **[OTf]**⁻ translocation. In other words, the time resolved Stokes shift during the anion translocation is similar to that of the solvent relaxation except that the temporal spectral evolution is much slower due to its translational type of motion. In a qualitative manner, we thus fit the resulting $C(t)$ by a single exponential decay function to extract the time constant. Note that a similar approach has been applied in theoretical studies on the solvation of the ion atmosphere (electrolyte solution)[52] and time-dependent Stokes shift experiments in ionic liquids.[47] For most studied compounds in toluene, we deconvoluted the temporal emission spectra with two Gaussian functions and used the lower energy emission peak as $\nu(t)$, and the longest wavelength emission peak in the steady-state emission spectrum was taken as $\nu(\infty)$. In this approach $\nu(0)$ is selected when the emergence of a spectral variation from F$_1$ to F$_2$ band is observed. Please see the ESI† for details of the fitting process. As a result, single exponential decay of $C(t)$ is observed for all studied compounds in toluene (see Fig. 2(b) for **2[OTf]**, **3[OTf]** and **4[OTf]** and Fig. S5(b)† for the remaining compounds). The fitted decay time constants are listed in Table 2. Clearly, the resulting time constants τ_{trans} are nearly parallel with those for rise components in the early dynamics obtained from the decay of emission monitored at a single wavelength (Table 2) with a single exponential decay fit. However, as mentioned, $C(t)$ is endowed with a more convincing physical meaning. Moreover, the standard deviation of the single exponential decay using $C(t)$ is smaller (*cf.* the decay at a selected emission wavelength). Hereafter, the time constant extracted from $C(t)$ is used to represent the translocation, denoted as τ_{trans}.

We next performed temperature dependent $C(t)$ measurements to probe if the process of anion translocation was associated with any energy barrier. In this approach, maintaining the viscosity during the measurement is crucial; otherwise, mixing "reaction barriers" and "viscosity mechanics barriers" will make data extraction too complex and unconvincing. To solve this hurdle, we employed a selection of weak polar solvents such as toluene, ethylbenzene, *n*-propylbenzene, cumene, and *sec*-butylbenzene at different temperatures. We have found that these weakly polar solvents have a minor effect on the emission peak wavelengths for the studied salts, and only alter the emission intensity ratio of F$_1$/F$_2$ due to different viscosities (Fig. S4†). We can thus achieve time traces of equal viscosity at different temperatures in corresponding solvents.[53] For example, at room temperature, we use *n*-propylbenzene as a solvent, while toluene is used as a solvent for the measurement at 267 K, *etc.* During the measurement, the viscosity was maintained between 0.84 and 0.86 centipoise (Table S9†). A detailed result of the temperature-dependent study using **3[OTf]** as the prototype is shown in Fig. S11.† We then applied the Arrhenius equation (eqn (2)) to extract the "activation energy" E_a.

$$\ln(k) = -\ln(\tau_{\text{trans}}) = \ln(\nu) - \frac{E_a}{RT} \qquad (2)$$

where k is the rate of anion translocation, which is inverse of τ_{trans}, R is the gas constant, T is the absolute temperature in Kelvin, and ν is the frequency factor. The plot shown in Fig. 3(a) gives an E_a value of 1.8 kcal mol^{-1} and a frequency factor of 10^{10} s^{-1}. The shallow barrier observed in **3[OTf]**, within experimental uncertainty, could be considered the same as the viscosity barrier reported for toluene of 2.2 kcal mol^{-1} (Fig. S13†).[54] The result suggests that, due to the diminished Coulomb interaction between the anion and the phosphonium acceptor in the excited state, the resistance of anion migration primarily comes from the surrounding solvents. Moreover, the low-frequency factor indicates that anion migration occurs *via* an intermolecular process between the anion and cation.[55] As a result, we deem the anion of the studied phosphonium salts essentially undergoes a barrierless motion, which gradually relaxes into a new form of ion pairs, *i.e.*, a different binding site, after ESICT.

Further support of the above viewpoint is given by the study of viscosity–translocation rate relationships for **3–7[OTf]** in weakly polar solvents at a constant temperature. This experiment was done by performing $C(t)$ measurement in toluene, ethylbenzene, *n*-propylbenzene, cumene, and *sec*-butylbenzene, which have similar polarities but different viscosities at room temperature (*vide supra*). As a result, the viscosity dependent rates extracted from $C(t)$ are listed in Fig. S6(a)–S10(a).† The obtained translocation rates are then fitted according to an empirical relation expressed in eqn (3) (ref. 7 and 56)

$$\ln(k) = -a \ln(\eta) + b \qquad (3)$$

where b is a viscosity-independent constant, η is the viscosity in centipoise (cP), and a is a characteristic factor that exhibits the correlation between translocation rate and viscosity, which is commonly in the range of 0–1. In theory, if there is no intrinsic barrier for the reaction, a is ∼1. As the intrinsic barrier increases, a decreases from 1 approaching 0.[7,57,58] The plot of eqn (3) for **3[OTf]** is shown in Fig. 3(b), while the results for other salts are presented in Fig. S7(b)–S10(b).† The plots all reveal a linear relationship with an a value of ∼1. We reaffirm that the anion translocation process primarily encounters friction from the surrounding solvents instead of the intrinsic barrier.

The slow anion translocation rate ($\tau_{\text{trans}} > 100$ ps) leads us to conclude that the anion migration mainly involves translational motion,[52,59] rather than the rotational diffusion that is dominant in the polar solvents. We then attempt to support the time domain of the anion migration with an anion drift model shown in Fig. 4 (see the explanation below).[60] The following equation is used to calculate the traveling time τ_{calc} required for an anion to arrive at the donor site

$$\tau_{\text{calc}} = \frac{L}{u \times |E_z|} \qquad (4)$$

where L is the traveling distance of the anion. For **3[OTf]** as an example, we define L as the distance between the phosphorus (orange) atom and nitrogen (blue) atom (see Fig. 4) which is calculated to be 10.3 Å. $|E_z|$ is the magnitude of electric field built due to the charge transfer between the acceptor and donor moiety along the z-axis direction; u is the mobility of **[OTf]**$^-$ and can be approximated based on Stokes' law (eqn (5))[61,62]

$$u = \frac{q}{6\pi\eta r} \qquad (5)$$

where q is the charge of mono-anion **[OTf]**$^-$, η is the viscosity of the surroundings (for example, toluene: 0.596 cP at 298 K, see Table S9†), and r is the radius of the anion (**[OTf]**$^-$: 2.48 Å (ref. 23)). It is worth mentioning that the Stokes–Einstein relation may not be valid when the interaction between the solute (here cations) and the solvent (here anions) is significant[63] owing to the ion pair formation. However, for translocation along the two terminal sites, the linear distance of **1–7** cationic backbones is evidently longer than that of **[OTf]**$^-$; therefore, our current fitted model provides acceptable results in a qualitative manner.

For **3[OTf]** and other phosphonium salts, the charge transfer cannot be 100% efficient, and the donor apparently acquires only a partial positive charge. In addition, neither an electron donor nor acceptor moiety is the point source of charge. To extract the effect of charge transfer, we then calculate the coulombic force exerted on the counter anion **[OTf]**$^-$, where
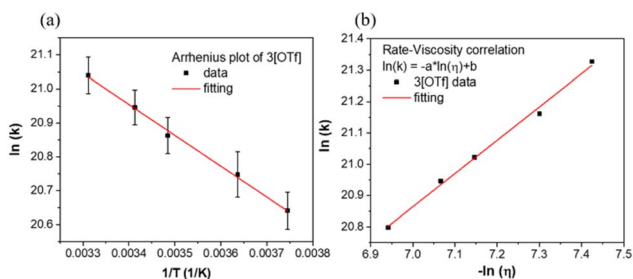

Fig. 3 (a) The plot of ln k, where k is the translocation rate, of **3[OTf]** anion migration as a function of $1/T$. (b) The plot of ln k of **3[OTf]** anion migration as a function of $-\ln \eta$ where η is the viscosity.
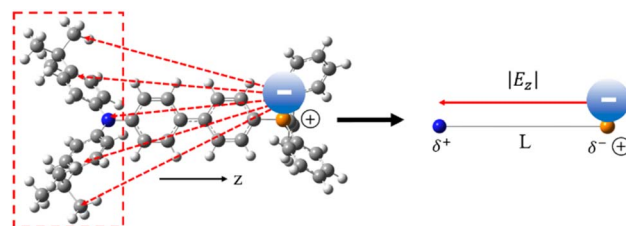

Fig. 4 Anion drift model used to calculate the traveling time of the anion to reach the donor. The time τ_{calc} required for the process is calculated by dividing the distance L from the phosphorus (orange) atom to the nitrogen (blue) atom by the product of the mobility u of the anion and the electric field $|E_z|$ along the z-axis between the donor and acceptor. For partial charge transfer cases (*e.g.*, **3[OTf]**), $|E_z|$ can be calculated using the restrained electrostatic potential (RESP) method on the S_1' state (see text for details).
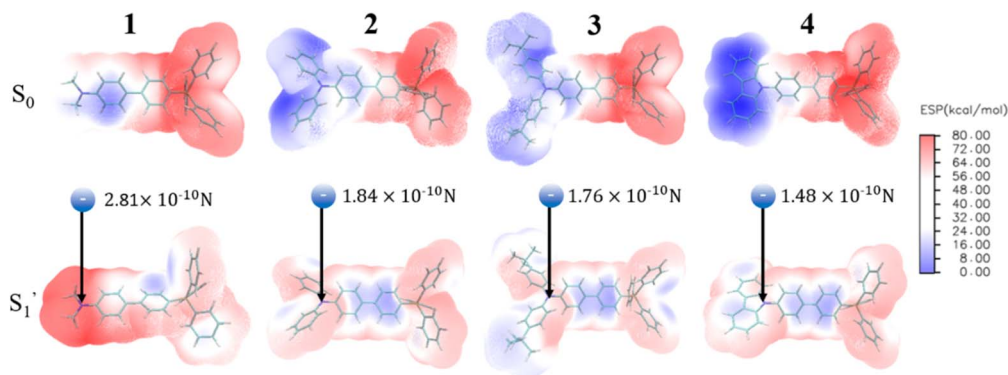
Fig. 5 Electrostatic potential (ESP) maps of the cations in group A calculated by the restrained electrostatic potential (RESP) method. The calculations are performed *via* Multiwfn program. We exhibit the net Coulomb interaction between the anion and donor moiety. The result will serve as an indicator of the degree of positive charge localization at the donor. (See the model in Fig. S18†).

each atom of the donor group has partial positive charge after ESICT, hence the sum of all the forces can be created. The atomic charge of each atom can be obtained by using the method of restrained electrostatic potential (RESP)[64,65] *via* the Multiwfn program,[66] where the calculation is performed under the geometry optimization of both ground (S_0) and relaxed excited states (S_1') without the anion using density functional theory (DFT) and time-dependent density functional theory (TDDFT), respectively (see ESI†). Fig. 5 depicts the calculated electrostatic potential (ESP) maps of cationic molecules **1–4** without anions and the results for the remaining studied molecules are shown in Fig. S16–S17.†

We next make the comparison between the experimentally resolved data τ_{trans} based on $C(t)$ and the theoretically derived τ_{calc} from eqn (4) where $|E_z|$ is obtained from the RESP method on the S_1' state. For the case of **3[OTf]**, τ_{calc} is derived to be 197 ps, which, in terms of magnitude, is close to the experimental result of τ_{trans} of 546 ps (see Fig. 2). In this theoretical approach, we overlook the overall charge distribution of the cation backbone after ESICT. Also, the Brownian motion cannot be simply described along the distance between the electron donor and acceptor. In other words, the calculated distance of 10.3 Å should be treated as a lower limit for distance, and the actual zigzag migration distance could be longer. Nevertheless, this simplified model provides an adequate magnitude of time scale for the photoinduced anion migration of the studied phosphonium salts.

Relation of donor–acceptor strength

Table 1 lists the calculated absorption and emission wavelengths of the studied compounds in toluene. The calculated values are consistent with the trend of the experimental data, giving us confidence in the use of HOMO/LUMO energy levels in discussing the corresponding donor/acceptor strength to the trend of anion migration rate. In theory, the HOMO with a higher energy level is expected to have stronger electron donating strength, which is calculated to be in the order of **2**(NPh$_2$)~**3**(N(*t*-BuPh)$_2$) > **1** (NMe$_2$) > **4**(carbazole) for group A (see Table 1). The calculated donor strength of **4** is obviously the weakest one in group A, which is consistent with the longest τ_{trans} (Table 2) experimentally measured. However, the donor strength of **1** should be at the third place, whereas its experimental τ_{trans} is the shortest in group A. This discrepancy can be rationalized by the structure *versus* electrostatic potential (Fig. 5). We may overlook the π-electron donating strength,[67,68] which involves orbital coupling between the electron donor and π-conjugated system. This coupling is weakened by simply increasing the dihedral angle between them. To examine the influence of dihedral angle on the π-electron donor strength, we then optimize both the structure of cations without anions in the S_0 state and S_1' state. We then define the dihedral angle between the donor plane and biphenyl bridge as θ_1, and the dihedral angle of the biphenyl group as θ_2 (see Table 3).

As shown in Table 3, after electron excitation, the cation backbone of groups A and B generally exhibits an increase in θ_1 from ∼30° to ∼40° and a decrease in θ_2 from ∼30° to ∼10°.[69–72] However, phosphonium **1** shows a distinct difference. Even after ESICT, **1** maintains θ_1 at 0°. This implies that the dimethyl amino group should be a stronger π-electron donor, which

Table 3 Dihedral angle of the cation of the phosphonium salts in toluene

	S_0		S_1'	
	θ_1 (°)	θ_2 (°)	θ_1 (°)	θ_2 (°)
1	0.16	33.19	0.19	15.69
2	31.37	34.32	39.93	11.24
3	29.92	33.20	41.79	12.41
4	51.25	38.22	46.77	0.42
5	30.12	33.39	40.07	11.82
6	31.57	48.24	39.65	29.48
7	30.75	20.38	38.22	14.77

would lead to prominent positive charge localization at the donor site in the excited state, giving the fastest anion migration among **1–4**. On the other hand, the lower energy of the LUMO points to a stronger electron acceptor strength that is anticipated to produce a more pronounced CT, *i.e.*, depletion of electron density from the donor. Consequently, the acceptor strength is $2(P^+Ph_3) > 5(P^+Cy_3)$ for group B, which is consistent with the significantly longer τ_{trans} of 1324 ps for **5[OTf]** than 258 ps for **2[OTf]**.

Group C that includes **2[OTf]**, **6[OTf]** and **7[OTf]** possesses the same electron donor and acceptor moieties, while an appreciable difference in anion migration rate is observed. Therefore, the dihedral angle θ_2 of the biphenyl spacer in the excited state might impact the dynamics within the ion pair. Both experimental and theoretical approaches indicate that **6 [OTf]** exhibits a faster translocation rate of $[OTf]^-$. The θ_2 of $\sim30°$ for the charge transfer state of **6** is more than twice larger than that of **2** and **7** (see the θ_2 values for the S_1' state in Table 3). Therefore, cation **6** retains the twisted structure after ESICT because of its methyl substituent. Consequently, the degree/efficiency of charge separation is better than that in **2** and **7**, which is reminiscent of the operation of twisted intramolecular charge transfer (TICT), facilitating charge separation.[72,73] This viewpoint is also verified by the ESP map of group C, where **6** in the S_1' state has more positive charge than that of **2** and **7** located at the donor site (Fig. S17†). Despite **2** and **7** both adopting a similar S_1' structure in terms of θ_1 and θ_2 (see Table 3), the electrostatic potential map of **7** indicates that the positive charge not only concentrates on the D–A sites, but also spreads across the biphenyl bridge due to the strictly locked framework in **7** (Fig. S17†), diminishing the positive charge built on the donor site. As a result, upon ESICT, the positive charge created in the donor site is in the order of $6 > 2 > 7$, which is consistent with the $(\tau_{trans})^{-1}$ of **6[OTf]** $(172\ ps)^{-1} > $ **2[OTf]** $(258\ ps)^{-1} > $ **7 [OTf]** $(467\ ps)^{-1}$.

Conclusions

In summary, we have designed a family of phosphonium fluorophores to investigate the kinetics of the ion migration processes, which occur upon excited-state charge transfer of ion pairs in weakly polar solvents. As the low polarity medium minimizes solvation of ionic species, the distinct spectral shift observed in the time-dependent emission spectra is mainly associated with the continuous translocation of the anion. Referring to the well-established solvatochromism, we found that anion migration shows similarities to solvent relaxation dynamics, except for the much slower time domain because of the involvement of anion translational motion. Based on this concept, we conducted in-depth studies on the anion migration dynamics of these phosphonium salts and put forward several remarks:

(1) We quantified the translocation rate by applying the spectral response function $C(t)$ and found that the spectral temporal evolution induced by anion translocation can be modeled using a mono-exponential decay kinetics. This property resembles the solvent relaxation but differs in the type of

motion involved. While the rotational diffusion dominates polar solvent relaxation (Debye–Onsager model), the anion migration is mainly governed by the translational motion through a distance and direction where the electric field is induced.

(2) The photoinduced anion translocation can be illustrated as a "migration" process with a negligible barrier, which is driven by the electric field built by charge transfer, as demonstrated by the viscosity and temperature dependent experiments. Note that the lack of an intrinsic barrier indicates that the friction imposed by the environment serves as a mechanical barrier to the migration.

(3) The velocity of anion translocation is proportional to the external electric field imposed by the positive charge temporarily located at the donor site upon charge transfer. Thus, we conclude that the rate of photoinduced anion migration is primarily governed by electrostatic interactions and charge redistribution.

From a microscopic point of view, the anion undergoes a biased Brownian motion along the pathway where the distance and direction are determined by the location and strength of electron donor and acceptor groups. Compared to the solvent relaxation with low viscosity, this migration process occurs at a much slower time scale, which is sensitive to the electric field created by ESICT.

Data availability

The data supporting this article have been included as part of the ESI.†

Author contributions

Conflicts of interest

There are no conflicts to declare.

Acknowledgements

Notes and references

1 X. Mao, M. Liu, Q. Li, C. Fan and X. Zuo, DNA-based molecular machines, *JACS Au*, 2022, **2**, 2381–2399.

2 H. Ramezani and H. Dietz, Building machines with DNA molecules, *Nat. Rev. Genet.*, 2020, **21**, 5–26.

3 W. R. Browne and B. L. Feringa, Making molecular machines work, *Nat. Nanotechnol.*, 2006, **1**, 25–35.

4 R. Iino, K. Kinbara and Z. Bryant, Introduction: molecular motors, *Chem. Rev.*, 2020, **120**, 1–4.

5 M. Xue, Y. Yang, X. Chi, X. Yan and F. Huang, Development of pseudorotaxanes and rotaxanes: from synthesis to stimuli–responsive motions to applications, *Chem. Rev.*, 2015, **115**, 7398–7501.

6 J. D. Badjic, C. M. Ronconi, J. F. Stoddart, V. Balzani, S. Silvi and A. Credi, Operating molecular elevators, *J. Am. Chem. Soc.*, 2006, **128**, 1489–1499.

7 D. C. Jagesar, S. M. Fazio, J. Taybi, E. Eiser, F. G. Gatti, D. A. Leigh and A. M. Brouwer, Photoinduced shuttling dynamics of rotaxanes in viscous polymer solutions, *Adv. Funct. Mater.*, 2009, **19**, 3440–3449.

8 I. Willner, V. Pardo-Yissar, E. Katz and K. T. Ranjit, A photoactivated 'molecular train' for optoelectronic applications: light-stimulated translocation of a β-cyclodextrin receptor within a stoppered azobenzene-alkyl chain supramolecular monolayer assembly on a Au-electrode, *J. Electroanal. Chem.*, 2001, **497**, 172–177.

9 D. W. Steuerman, H.-R. Tseng, A. J. Peters, A. H. Flood, J. O. Jeppesen, K. A. Nielsen, J. F. Stoddart and J. R. Heath, Molecular-mechanical switch-based solid-state electrochromic devices, *Angew. Chem., Int. Ed.*, 2004, **43**, 6486–6491.

10 C. Kwamen and J. Niemeyer, Functional rotaxanes in catalysis, *Chem.–Eur. J.*, 2021, **27**, 175–186.

11 M. J. Langton and P. D. Beer, Rotaxane and catenane host structures for sensing charged guest species, *Acc. Chem. Res.*, 2014, **47**, 1935–1949.

12 N. Pairault, R. Barat, I. Tranoy-Opalinski, B. Renoux, M. Thomas and S. Papot, Rotaxane-based architectures for biological applications, *C. R. Chim.*, 2016, **19**, 103–112.

13 B. Yao, H. Sun, L. Yang, S. Wang and X. Liu, Recent progress in light-driven molecular shuttles, *Front. Chem.*, 2022, **9**, 832735.

14 P. Wu, B. Dharmadhikari, P. Patra and X. Xiong, Rotaxane nanomachines in future molecular electronics, *Nanoscale Adv.*, 2022, **4**, 3418–3461.

15 M. N. Chatterjee, E. R. Kay and D. A. Leigh, Beyond switches: ratcheting a particle energetically uphill with a compartmentalized molecular machine, *J. Am. Chem. Soc.*, 2006, **128**, 4058–4073.

16 S. Erbas-Cakmak, D. A. Leigh, C. T. McTernan and A. L. Nussbaumer, Artificial molecular machines, *Chem. Rev.*, 2015, **115**, 10081–10206.

17 V. Balzani, A. Credi and M. Venturi, Light powered molecular machines, *Chem. Soc. Rev.*, 2009, **38**, 1542–1550.

18 H. Tian and Q.-C. Wang, Recent progress on switchable rotaxanes, *Chem. Soc. Rev.*, 2006, **35**, 361–374.

19 S. Garaudée, S. Silvi, M. Venturi, A. Credi, A. H. Flood and J. F. Stoddart, Shuttling Dynamics in an Acid–Base-Switchable [2] Rotaxane, *ChemPhysChem*, 2005, **6**, 2145–2152.

20 A. S. Lane, D. A. Leigh and A. Murphy, Peptide-based molecular shuttles, *J. Am. Chem. Soc.*, 1997, **119**, 11092–11093.

21 M. R. Panman, P. Bodis, D. J. Shaw, B. H. Bakker, A. C. Newton, E. R. Kay, A. M. Brouwer, W. J. Buma, D. A. Leigh and S. Woutersen, Operation mechanism of a molecular machine revealed using time-resolved vibrational spectroscopy, *Science*, 2010, **328**, 1255–1258.

22 A. M. Brouwer, C. Frochot, F. G. Gatti, D. A. Leigh, L. Mottier, F. Paolucci, S. Roffia and G. W. Wurpel, Photoinduction of fast, reversible translational motion in a hydrogen-bonded molecular shuttle, *Science*, 2001, **291**, 2124–2128.

23 A. Belyaev, Y. H. Cheng, Z. Y. Liu, A. J. Karttunen, P. T. Chou and I. O. Koshevoy, A Facile Molecular Machine: Optically Triggered Counterion Migration by Charge Transfer of Linear Donor-π-Acceptor Phosphonium Fluorophores, *Angew. Chem., Int. Ed.*, 2019, **58**, 13456–13465.

24 T.-C. Lin, Z.-Y. Liu, S.-H. Liu, I. O. Koshevoy and P.-T. Chou, Counterion migration driven by light-induced intramolecular charge transfer, *JACS Au*, 2021, **1**, 282–293.

25 A. Belyaev, B. K. Su, Y. H. Cheng, Z. Y. Liu, N. M. Khan, A. J. Karttunen, P. T. Chou and I. O. Koshevoy, Multiple Emission of Phosphonium Fluorophores Harnessed by the Pathways of Photoinduced Counterion Migration, *Angew. Chem.*, 2022, **134**, e202115690.

26 K. H. Chang, Y. H. Yang, K. H. Su, Y. Chen, T. C. Lin, J. L. Li, Z. Y. Liu, J. H. Shi, T. F. Wang and Y. T. Chang, Light Induced Proton Coupled Charge Transfer Triggers Counterion Directional Translocation, *Angew. Chem., Int. Ed.*, 2024, e202403317.

27 V. Balzani, M. Clemente-Leon, A. Credi, B. Ferrer, M. Venturi, A. H. Flood and J. F. Stoddart, Autonomous artificial nanomotor powered by sunlight, *Proc. Natl. Acad. Sci. U. S. A.*, 2006, **103**, 1178–1183.

28 L. Tang, Concentration dependence of diffusion and migration of chloride ions Part 1. Theoretical considerations, *Cem. Concr. Res.*, 1999, 1463–1468.

29 D. Marcoux and A. B. Charette, Nickel-Catalyzed Synthesis of Phosphonium Salts from Aryl Halides and Triphenylphosphine, *Adv. Synth. Catal.*, 2008, **350**, 2967–2974.

30 S. Cha, M. G. Choi, H. R. Jeon and S.-K. Chang, Negative solvatochromism of merocyanine dyes: Application as water content probes for organic solvents, *Sens. Actuators, B*, 2011, **157**, 14–18.

31 A. V. Kulinich, E. K. Mikitenko and A. A. Ishchenko, Scope of negative solvatochromism and solvatofluorochromism of merocyanines, *Phys. Chem. Chem. Phys.*, 2016, **18**, 3444–3453.

32 P. Fromherz, Monopole-dipole model for symmetrical solvatochromism of hemicyanine dyes, *J. Phys. Chem.*, 1995, **99**, 7188–7192.

33 D. Laage, W. H. Thompson, M. Blanchard-Desce and J. T. Hynes, Charged push–pull polyenes in solution: anomalous solvatochromism and nonlinear optical properties, *J. Phys. Chem. A*, 2003, **107**, 6032–6046.

34 B. Carlotti, G. Consiglio, F. Elisei, C. G. Fortuna, U. Mazzucato and A. Spalletti, Intramolecular charge transfer of push–pull pyridinium salts in the singlet manifold, *J. Phys. Chem. A*, 2014, **118**, 3580–3592.

35 B. Carlotti, A. Cesaretti, C. Fortuna, A. Spalletti and F. Elisei, Experimental evidence of dual emission in a negatively solvatochromic push–pull pyridinium derivative, *Phys. Chem. Chem. Phys.*, 2015, **17**, 1877–1882.

36 B. Carlotti, E. Benassi, V. Barone, G. Consiglio, F. Elisei, A. Mazzoli and A. Spalletti, Effect of the π Bridge and Acceptor on Intramolecular Charge Transfer in Push–Pull Cationic Chromophores: An Ultrafast Spectroscopic and TD-DFT Computational Study, *ChemPhysChem*, 2015, **16**, 1440–1450.

37 S. Nigam and S. Rutan, Principles and applications of solvatochromism, *Appl. Spectrosc.*, 2001, **55**, 362A–370A.

38 Z. Liu, T. Lu and Q. Chen, An sp-hybridized all-carboatomic ring, cyclo [18] carbon: electronic structure, electronic spectrum, and optical nonlinearity, *Carbon*, 2020, **165**, 461–467.

39 Y. Zhao and D. G. Truhlar, The M06 suite of density functionals for main group thermochemistry, thermochemical kinetics, noncovalent interactions, excited states, and transition elements: two new functionals and systematic testing of four M06-class functionals and 12 other functionals, *Theor. Chem. Acc.*, 2008, **120**, 215–241.

40 W. J. Hehre, R. Ditchfield and J. A. Pople, Self—consistent molecular orbital methods. XII. Further extensions of Gaussian—type basis sets for use in molecular orbital studies of organic molecules, *J. Chem. Phys.*, 1972, **56**, 2257–2261.

41 A. Koti, M. Krishna and N. Periasamy, Time-resolved area-normalized emission spectroscopy (TRANES): a novel method for confirming emission from two excited states, *J. Phys. Chem. A*, 2001, **105**, 1767–1771.

42 G. van der Zwan and J. T. Hynes, Time-dependent fluorescence solvent shifts, dielectric friction, and nonequilibrium solvation in polar solvents, *J. Phys. Chem.*, 1985, **89**, 4181–4188.

43 J. D. Simon, Time-resolved studies of solvation in polar media, *Acc. Chem. Res.*, 1988, **21**, 128–134.

44 M. Maroncelli, The dynamics of solvation in polar liquids, *J. Mol. Liq.*, 1993, **57**, 1–37.

45 V. Nagarajan, A. M. Brearley, T. J. Kang and P. F. Barbara, Time-resolved spectroscopic measurements on microscopic solvation dynamics, *J. Chem. Phys.*, 1987, **86**, 3183–3196.

46 J. D. Simon and S. G. Su, Intramolecular electron transfer and solvation, *J. Chem. Phys.*, 1987, **87**, 7016–7023.

47 C. F. Chapman and M. Maroncelli, Fluorescence studies of solvation and solvation dynamics in ionic solutions, *J. Phys. Chem.*, 1991, **95**, 9095–9114.

48 M. Horng, J. Gardecki, A. Papazyan and M. Maroncelli, Subpicosecond measurements of polar solvation dynamics: coumarin 153 revisited, *J. Phys. Chem.*, 1995, **99**, 17311–17337.

49 A. P. Demchenko, K.-C. Tang and P.-T. Chou, Excited-state proton coupled charge transfer modulated by molecular structure and media polarization, *Chem. Soc. Rev.*, 2013, **42**, 1379–1408.

50 T. Kumpulainen, B. Lang, A. Rosspeintner and E. Vauthey, Ultrafast elementary photochemical processes of organic molecules in liquid solution, *Chem. Rev.*, 2017, **117**, 10826–10939.

51 S.-G. S. a. J. D. Simon, Importance of Molecular Size on the Dynamics of Solvent Relaxation, *J. Phys. Chem.*, 1989, **93**, 753–758.

52 G. van der Zwan and J. T. Hynes, Chemical reaction rates and solvation dynamics in electrolyte solutions: ion atmosphere friction, *Chem. Phys.*, 1991, **152**, 169–183.

53 A. Barlow, J. Lamb and A. Matheson, Viscous behaviour of supercooled liquids, *Proc. Roy. Soc. Lond. Math. Phys. Sci.*, 1966, **292**, 322–342.

54 K. R. Harris, Temperature and density dependence of the viscosity of toluene, *J. Chem. Eng. Data*, 2000, **45**, 893–897.

55 J. Syage, P. Felker and A. Zewail, Picosecond excitation and selective intramolecular rates in supersonic molecular beams. III. Photochemistry and rates of a charge transfer reaction, *J. Chem. Phys.*, 1984, **81**, 2233–2256.

56 S. H. Courtney and G. R. Fleming, Search for the kramers theory turnover: photochemical isomerization at very low viscosities, *Chem. Phys. Lett.*, 1984, **103**, 443–446.

57 R. K. Murarka, S. Bhattacharyya, R. Biswas and B. Bagchi, Isomerization dynamics in viscous liquids: microscopic investigation of the coupling and decoupling of the rate to and from solvent viscosity and dependence on the intermolecular potential, *J. Chem. Phys.*, 1999, **110**, 7365–7375.

58 H. Sumi, Theory on reaction rates in nonthermalized steady states during conformational fluctuations in viscous solvents, *J. Phys. Chem.*, 1991, **95**, 3334–3350.

59 G. Ciccotti, M. Ferrario, J. T. Hynes and R. Kapral, Dynamics of ion pair interconversion in a polar solvent, *J. Chem. Phys.*, 1990, **93**, 7137–7147.

60 V. Gabelica and E. Marklund, Fundamentals of ion mobility spectrometry, *Curr. Opin. Chem. Biol.*, 2018, **42**, 51–59.

61 C. Larriba-Andaluz and F. Carbone, The size-mobility relationship of ions, aerosols, and other charged particle matter, *J. Aerosol Sci.*, 2021, **151**, 105659.

62 J. T. Edward, Molecular volumes and the Stokes–Einstein equation, *J. Chem. Educ.*, 1970, **47**, 261.

63 P. Banerjee and B. Bagchi, Role of local order in anomalous ion diffusion: Interrogation through tetrahedral entropy of aqueous solvation shells, *J. Chem. Phys.*, 2020, **153**, 154505.

64 J. Zhang and T. Lu, Efficient evaluation of electrostatic potential with computerized optimized code, *Phys. Chem. Chem. Phys.*, 2021, **23**, 20323–20328.

65 C. I. Bayly, P. Cieplak, W. Cornell and P. A. Kollman, A well-behaved electrostatic potential based method using charge restraints for deriving atomic charges: the RESP model, *J. Phys. Chem.*, 1993, **97**, 10269–10280.

66 T. Lu and F. Chen, Multiwfn: a multifunctional wavefunction analyzer, *J. Comput. Chem.*, 2012, **33**, 580–592.

67 O. Kwon, S. Barlow, S. A. Odom, L. Beverina, N. J. Thompson, E. Zojer, J.-L. Brédas and S. R. Marder, Aromatic amines: a comparison of electron-donor strengths, *J. Phys. Chem. A*, 2005, **109**, 9346–9352.

68 P. Hrobarik, I. Sigmundova, P. Zahradnik, P. Kasak, V. Arion, E. Franz and K. Clays, Molecular engineering of benzothiazolium salts with large quadratic hyperpolarizabilities: can auxiliary electron-withdrawing groups enhance nonlinear optical responses?, *J. Phys. Chem. C*, 2010, **114**, 22289–22302.

69 M. Maus and W. Rettig, The electronic structure of 4-(*N*,*N*-dimethylamino)-4′-cyano-biphenyl and its planar and twisted model compounds, *Chem. Phys.*, 1997, **218**, 151–162.

70 M. Maus, W. Rettig, G. Jonusauskas, R. Lapouyade and C. Rullière, Subpicosecond transient absorption of donor–acceptor biphenyls. Intramolecular control of the excited state charge transfer processes by a weak electronic coupling, *J. Phys. Chem. A*, 1998, **102**, 7393–7405.

71 M. Maus, W. Rettig, D. Bonafoux and R. Lapouyade, Photoinduced intramolecular charge transfer in a series of differently twisted donor–acceptor biphenyls as revealed by fluorescence, *J. Phys. Chem. A*, 1999, **103**, 3388–3401.

72 R. Ghosh, A. Nandi and D. K. Palit, Solvent sensitive intramolecular charge transfer dynamics in the excited states of 4-*N*,*N*-dimethylamino-4′-nitrobiphenyl, *Phys. Chem. Chem. Phys.*, 2016, **18**, 7661–7671.

73 Z. R. Grabowski, K. Rotkiewicz and W. Rettig, Structural changes accompanying intramolecular electron transfer: focus on twisted intramolecular charge-transfer states and structures, *Chem. Rev.*, 2003, **103**, 3899–4032.